

Molecular Hydrogen: a benchmark system for Near Threshold Resonances at higher partial waves

D. Shu, I. Simbotin, R. Côté
University of Connecticut, Storrs, CT 06268, USA

Benchmark reactions involving molecular hydrogen, such as H_2+D or H_2+Cl , provide the ideal platforms to investigate the effect of Near Threshold Resonances (NTR) on scattering processes. Due to the small reduced mass of those systems, shape resonances due to particular partial waves can provide features at scattering energies up to a few Kelvins, reachable in recent experiments. We explore the effect of NTRs on elastic and inelastic scattering for higher partial waves ℓ in the case of H_2+Cl for s -wave and H_2+D for p -wave scattering, and find that NTRs lead to a different energy scaling of the cross sections as compared to the well known Wigner threshold regime. We give a theoretical analysis based on Jost functions for short range interaction potentials. To explore higher partial waves, we adopt a three channel model that incorporates all key ingredients, and explore how the NTR scaling is affected by ℓ . A short discussion on the effect of the long-range form of the interaction potential is also provided.

PACS numbers:

I. INTRODUCTION

Atomic and molecular hydrogen are the most abundant, and in many ways the most fundamental, constituents of matter in the universe. For example, reactions such as $\text{H}_2+\text{D}\rightarrow\text{HD}+\text{H}$ are relevant to astrophysics, especially for the astrochemistry in the early universe [1] and the evolution of cold molecular clouds in the earliest stages of star formation [2]. In addition, hydrogen is the perfect system to test our theoretical understanding by allowing high precision calculations. In particular, basic chemical systems involving molecular hydrogen, such as H_2+D , H_2+Cl , or H_2+F , provide benchmark systems for which potential energy surfaces (PES) can be calculated to a high level of accuracy.

Another fundamental feature in scattering are resonances. They are ubiquitous, appearing as potential or shape resonance, or as Feshbach resonances. Although their effect is often averaged over at room or higher temperatures, they can become the dominant feature at low or ultralow temperatures, where only a few partial waves might contribute to the scattering process. Since cold molecules were first predicted [3, 4] and observed experimentally [5, 6], rapid progress has been made in our ability to form and manipulate ultracold molecules [7, 8], which provides the seed to study in a precise and controlled fashion [9] the role of single partial waves, and state-to-state processes [10] in chemical systems. In fact, early experiments on KRb ultracold molecules [11, 12], which explored quantum-state controlled chemical reactions using quantum statistics, motivated several studies of chemical systems under extreme conditions, and particularly the role of resonances in controlling the outcome. This high level of control over interactions can be realized using Feshbach resonances [13], or by orienting ultracold molecules [14, 15]. In addition to investigations of degenerate quantum gases [16, 17], such control also allows studies of exotic three-body Efimov states [18, 19] or application to quantum information processing [20–22].

In previous work, we have studied ultracold reactions involving molecular hydrogen, such as H_2+D [23–25] H_2+Cl [26, 27] and H_2+F [27]. We also showed that shape resonances due to higher partial waves appear in certain reaction channels in H_2+D [24, 25] and D_2+H [28]. Due to the small reduced mass of these systems and shallow van der Waals complexes, these resonances occur at scattering energies corresponding to a few mK up to a few K, *i.e.* above the “standard” ultracold regime usually nearing μK . Similar resonances were recently observed in H_2 scattering with He^* (metastable helium) [29–32]. Such studies of benchmark reactions involving H_2 should lead to a better understanding of the energy surface and of the relevant scattering processes.

Previously, we explored the effect of near-threshold resonances on reaction rates in H_2+Cl and H_2+F [26, 27] for the ultracold case where only the s -wave contribution plays a role. In this article, we extend our analysis to higher partial waves; for $\ell \geq 2$, we employ a model based on three coupled open channels that incorporates the key ingredients while allowing for easy tuning of the resonances for each partial wave ℓ . We uncover specific scaling differing from the expected Wigner’s scaling laws for given partial waves ℓ .

We first review scattering theory for multi-channel problems to establish the notation, followed by the corresponding Jost function treatment. Using mass scaling, we demonstrate how near threshold resonances (NTRs) manifest themselves in H_2+Cl ($\ell = 0$) and H_2+D ($\ell = 1$). We build on the Jost function approach to formulate the NTR regime scaling laws, and illustrate them with the simpler model for $\ell \geq 2$. We finally discuss briefly the effect of a power-law potential tail on those scalings.

II. SCATTERING

In a multichannel scattering problem, the scattering wave function $\psi_{\mathbf{k}}^+$ for an incident projectile with momen-

tum $\mathbf{p} = \hbar\mathbf{k}$ can be expanded onto a complete basis representing the channels. Here, we review the case of non-reactive processes, where the initial arrangement remains intact after the scattering event, though the general results are applicable to the reactive case. A more thorough discussion can be found in several scattering textbooks, such as [33–35].

Below, we limit our discussion to the non-reactive case (although the results can be generalized to the rearrangement case [33]), and assume the Hamiltonian

$$\hat{H} = \left(\frac{\mathbf{p}^2}{2\mu} + \hat{H}_{\text{target}} \right) + V(\mathbf{r}, \mathbf{s}), \quad (1)$$

where \mathbf{r} is the position projectile and \mathbf{s} the set of coordinates describing the target, μ is the reduced mass of the projectile and target, and $V(\mathbf{r}, \mathbf{s})$ the interaction between them. Here, \hat{H}_{target} dictates the target dynamics, with $\hat{H}_{\text{target}}\phi_n(\mathbf{s}) = E_n\phi_n(\mathbf{s})$. We expand $\psi_{\mathbf{k}}^+(k, \mathbf{r}, \mathbf{s})$ in the basis of $\phi_n(\mathbf{s})$, *i.e.*

$$\psi_{\mathbf{k}}^+(k, \mathbf{r}, \mathbf{s}) = \sum_n \eta_n(\mathbf{r})\phi_n(\mathbf{s}), \quad (2)$$

where $\eta_n(\mathbf{r})$ correspond to the channel wave functions, and the sum runs over discrete and continuum states. Their asymptotic form is written as

$$\eta_n(\mathbf{r}) \xrightarrow{r \rightarrow \infty} \delta_{ni} e^{i\mathbf{k} \cdot \mathbf{r}} + f_{ni} \frac{e^{ik_n r}}{r}, \quad (3)$$

where $f_{ni} \equiv f(\mathbf{k}_n, n \leftarrow \mathbf{k}, i)$ stands for the scattering amplitude from the initial/incident channel i with momentum $\mathbf{p} = \hbar\mathbf{k}$ into the channel n with momentum $\mathbf{p}_n = \hbar\mathbf{k}_n$.

Applying \hat{H} onto the expansion (2) for $\psi_{\mathbf{k}}^+(k, \mathbf{r}, \mathbf{s})$, and using orthonormality $\int d\mathbf{s} \phi_m^*(\mathbf{s})\phi_n(\mathbf{s}) = \delta_{mn}$, of the basis ϕ_n , one gets [33]

$$-\frac{\hbar^2 \nabla^2}{2\mu} \eta_m(\mathbf{r}) + \sum_n V_{mn}(\mathbf{r}) \eta_n(\mathbf{r}) = (E - E_m) \eta_m(\mathbf{r}), \quad (4)$$

where

$$V_{mn}(\mathbf{r}) \equiv \int d\mathbf{s} \phi_m^*(\mathbf{s}) V(\mathbf{r}, \mathbf{s}) \phi_n(\mathbf{s}). \quad (5)$$

Although there is in principle an infinite set of coupled equations due to the infinite number of states arising from the continuum, one generally neglects its contribution and restricts the number N of discrete terms considered to obtain *the close-coupling approximation*.

In that case, if we label the initial/incident channel by $i = 1$, the solution $\boldsymbol{\eta}_1(\mathbf{r})$ of the scattering problem, Eq.(4), can be rewritten in the matrix form

$$\nabla^2 \boldsymbol{\eta}_1(\mathbf{r}) - \mathbf{U}(\mathbf{r}) \boldsymbol{\eta}_1(\mathbf{r}) + \mathbf{K}^2 \boldsymbol{\eta}_1(\mathbf{r}) = 0, \quad (6)$$

where

$$\boldsymbol{\eta}_1(\mathbf{r}) = \begin{pmatrix} \eta_{i=1}(\mathbf{r}) \\ \vdots \\ \eta_N(\mathbf{r}) \end{pmatrix}, \quad \mathbf{K} = \begin{pmatrix} k_1 & & 0 \\ & \ddots & \\ 0 & & k_N \end{pmatrix}, \quad (7)$$

with $k_n = \sqrt{2\mu(E - E_n)/\hbar^2}$, and where $\mathbf{U}(\mathbf{r})$ is a $N \times N$ matrix with elements $U_{mn} = \frac{2m}{\hbar^2} V_{mn}$. In general, the incident wave can be in any of the channels $n = 1, \dots, N$, leading to N distinct solutions $\boldsymbol{\eta}_1(\mathbf{r}), \dots, \boldsymbol{\eta}_N(\mathbf{r})$, where each $\boldsymbol{\eta}_n(\mathbf{r})$ describes a collision beginning in channel $i = n$, so that Eq.(6) can be rewritten as

$$\nabla^2 \bar{\boldsymbol{\eta}}(\mathbf{r}) - \mathbf{U}(\mathbf{r}) \bar{\boldsymbol{\eta}}(\mathbf{r}) + \mathbf{K}^2 \bar{\boldsymbol{\eta}}(\mathbf{r}) = 0, \quad (8)$$

where $\bar{\boldsymbol{\eta}}(\mathbf{r})$ is a matrix with each column being the solution for an initial channel

$$\bar{\boldsymbol{\eta}}(\mathbf{r}) = (\boldsymbol{\eta}_1(\mathbf{r}), \boldsymbol{\eta}_2(\mathbf{r}), \dots, \boldsymbol{\eta}_N(\mathbf{r})), \quad (9)$$

with

$$\boldsymbol{\eta}_1 = \begin{pmatrix} \eta_{i=1} \\ \eta_2 \\ \vdots \\ \eta_N \end{pmatrix}, \quad \boldsymbol{\eta}_2 = \begin{pmatrix} \eta_1 \\ \eta_{i=2} \\ \vdots \\ \eta_N \end{pmatrix}, \quad \dots, \quad \boldsymbol{\eta}_N = \begin{pmatrix} \eta_1 \\ \eta_2 \\ \vdots \\ \eta_{i=N} \end{pmatrix}. \quad (10)$$

We consider the case where the system is rotationally invariant and spinless, so that the solutions $\boldsymbol{\eta}_n(\mathbf{r})$ can be written in a partial wave expansion of the form [33]

$$\boldsymbol{\eta}_n(\mathbf{r}) = \sum_{\ell=0}^{\infty} \frac{(2\ell+1)}{kr} \boldsymbol{\psi}_n^{(\ell)}(r) P_{\ell}(\cos\theta), \quad (11)$$

which satisfies the matrix radial equation

$$\left[\mathbf{I} \frac{d^2}{dr^2} - \mathbf{I} \frac{\ell(\ell+1)}{r^2} - \mathbf{U}(r) + \mathbf{K}^2 \right] \boldsymbol{\psi}_n^{(\ell)}(r) = 0. \quad (12)$$

The vector $\boldsymbol{\psi}_n^{(\ell)}(r)$ is the radial solution with the incident wave in channel $i = n$, and for each angular momentum ℓ , there are N distinct radial functions $\boldsymbol{\psi}_n^{(\ell)}(r)$. Each vector $\boldsymbol{\psi}_n^{(\ell)}(r)$ has N components $\psi_{mn}^{(\ell)}(r)$, and their asymptotic form is given by

$$\begin{aligned} \psi_{mn}^{(\ell)}(r) &\xrightarrow{r \rightarrow \infty} C(k_n) \left[i^{\ell} s_{\ell}(k_n r) \delta_{mn} + k_n f_{mn}^{(\ell)} e^{ik_m r} \right] \\ &= C(k_n) \frac{i^{2\ell+1}}{2} \left[e^{-ik_n r} \delta_{mn} \right. \\ &\quad \left. - (-1)^{\ell} \sqrt{\frac{k_n}{k_m}} S_{mn}^{(\ell)} e^{ik_m r} \right], \end{aligned} \quad (13)$$

where $s_{\ell}(x) = x j_{\ell}(x)$ is the Riccati-Bessel function, $C(k_n)$ is a normalization constant, and where $f_{mn}^{(\ell)}$ and $S_{mn}^{(\ell)}$ are related by

$$S_{mn}^{(\ell)} = \delta_{mn} + 2i \sqrt{k_m k_n} f_{mn}^{(\ell)}. \quad (14)$$

The $\sqrt{k_n/k_m}$ factor appearing with $S_{mn}^{(\ell)}$ in Eq.(13) ensures the unitarity of the S-matrix.

Regrouping all vectors $\psi_n^{(\ell)}(r)$ into a single $N \times N$ matrix as for $\bar{\eta}(\mathbf{r})$ in Eq.(9), we have

$$\bar{\Psi}^{(\ell)}(r) = (\psi_1^{(\ell)}(r), \psi_2^{(\ell)}(r), \dots, \psi_N^{(\ell)}(r)), \quad (15)$$

and the asymptotic forms in Eq.(13) are rewritten as

$$\begin{aligned} \bar{\Psi}^{(\ell)}(r) &\xrightarrow{r \rightarrow \infty} \left[i^\ell s_\ell(\mathbf{K}r) + e^{i\mathbf{K}r} \mathbf{F}^{(\ell)} \mathbf{K} \right] C(\mathbf{K}) \\ &= \frac{i^{2\ell+1}}{2} \left[e^{-i\mathbf{K}r} - (-1)^\ell e^{i\mathbf{K}r} \mathbf{K}^{-1/2} \mathbf{S}^{(\ell)} \mathbf{K}^{1/2} \right] C(\mathbf{K}), \end{aligned} \quad (16)$$

where $\mathbf{F}^{(\ell)}$ and $\mathbf{S}^{(\ell)}$ are the matrices for $f_{mn}^{(\ell)}$ and $S_{mn}^{(\ell)}$, \mathbf{K} given in Eq.(7) with $\mathbf{K}^{\pm 1/2} = \text{diag}\{k_j^{\pm 1/2}\}$, and with the various diagonal matrices defined as $C(\mathbf{K}) = \text{diag}\{C(k_j)\}$, $s_\ell(\mathbf{K}r) = \text{diag}\{s_\ell(k_j r)\}$, and $e^{\pm i\mathbf{K}r} = \text{diag}\{e^{\pm ik_j r}\}$. Eq.(14) is then written as

$$\mathbf{S}^{(\ell)} = \mathbf{I} + 2i\mathbf{K}^{1/2} \mathbf{F}^{(\ell)} \mathbf{K}^{1/2}. \quad (17)$$

The order of the matrix multiplication is important in those matrix forms.

Differential cross sections for multi-channel scattering with and without rearrangement are given by [33]

$$\frac{d\sigma_{m \leftarrow n}}{d\Omega} = \frac{k_m}{k_n} |f_{mn}|^2, \quad (18)$$

In general, the exact form of the expression depends on the angular momenta, internal structure, and the exact interactions entering the Hamiltonian (such as interaction with external fields, etc.). For the simpler rotationally invariant and spinless system satisfying Eqs.(11) and (12), we have

$$f_{mn} = \sum_{\ell=0}^{\infty} (2\ell+1) f_{mn}^{(\ell)} P_\ell(\cos \theta). \quad (19)$$

Using the properties of Legendre polynomials P_ℓ , and after integration over angles, one gets

$$\sigma_{m \leftarrow n}(k_n) = 4\pi \frac{k_m}{k_n} \sum_{\ell=0}^{\infty} (2\ell+1) |f_{mn}^{(\ell)}|^2, \quad (20)$$

which can be rewritten, with the help of Eq.(14), as

$$\sigma_{m \leftarrow n}(k_n) = \frac{\pi}{k_n^2} \sum_{\ell=0}^{\infty} (2\ell+1) |\delta_{mn} - S_{mn}^{(\ell)}|^2, \quad (21)$$

$$= \frac{\pi}{k_n^2} \sum_{\ell=0}^{\infty} (2\ell+1) |T_{mn}^{(\ell)}|^2, \quad (22)$$

$$= \sum_{\ell=0}^{\infty} (2\ell+1) \sigma_{m \leftarrow n}^{(\ell)}(k_n), \quad (23)$$

where we define the partial cross section $\sigma_{m \leftarrow n}^{(\ell)}(k_n)$ in term of the T-matrix, namely

$$\sigma_{m \leftarrow n}^{(\ell)}(k_n) \equiv \frac{\pi}{k_n^2} |T_{mn}^{(\ell)}|^2. \quad (24)$$

The T-matrix $T_{mn}^{(\ell)} = \delta_{mn} - S_{mn}^{(\ell)}$ can be written as

$$\mathbf{T} = \mathbf{I} - \mathbf{S}. \quad (25)$$

Using the unitarity of the S-matrix, namely $1 = \sum_m |S_{mn}^{(\ell)}|^2 = |S_{nn}^{(\ell)}|^2 + \sum_{m \neq n} |S_{mn}^{(\ell)}|^2$, the elastic and total inelastic cross sections are simply

$$\sigma_n^{\text{elas}} \equiv \sigma_{n \leftarrow n} = \frac{\pi}{k_n^2} \sum_{\ell=0}^{\infty} (2\ell+1) |S_{nn}^{(\ell)}|^2, \quad (26)$$

$$\sigma_n^{\text{inel}} \equiv \sum_{m \neq n} \sigma_{m \leftarrow n} = \frac{\pi}{k_n^2} \sum_{\ell=0}^{\infty} (2\ell+1) [1 - |S_{nn}^{(\ell)}|^2]. \quad (27)$$

We note that in the zero-energy limit, the cross sections are given by the s -wave ($\ell=0$) partial wave and can be expressed in terms of a complex scattering length $a_n = \alpha_n - i\beta_n$ [26, 36], namely $\sigma_n^{\text{elas}} \sim 4\pi|a_n|^2$ and $\sigma_n^{\text{inel}} \sim 4\pi\beta_n/k_n$, which exemplify the usual Wigner's threshold regime [26, 36, 37].

Resonances can be understood from the appearance of poles in the structure of the S-matrix, and the proximity of the scattering energy E (or momentum k) from these poles. A useful formalism to explore these effect is based on the Jost function.

III. JOST FUNCTION

We consider rotationally invariant and spinless systems. For N coupled channels, the regular solution $\bar{\phi}^{(\ell)}(r)$ is an $N \times N$ matrix with elements $\phi_{mn}^{(\ell)}$ satisfying the system of coupled radial equations,

$$\mathbf{I} \frac{d^2}{dr^2} \bar{\phi}^{(\ell)}(r) = \left[\mathbf{U}(r) + \mathbf{I} \frac{\ell(\ell+1)}{r^2} - \mathbf{K}^2 \right] \bar{\phi}^{(\ell)}(r). \quad (28)$$

The element $\phi_{mn}^{(\ell)}$ must satisfy the boundary condition $\phi_{mn}^{(\ell)}(r) \sim \delta_{mn}(k_n r)^{\ell+1}$ as $r \rightarrow 0$. For potential elements U_{mn} less singular than r^{-2} at the origin and vanishing faster than r^{-3} at ∞ , the asymptotic behavior of $\phi_{mn}^{(\ell)}$ can be written as

$$\phi_{mn}^{(\ell)}(r) \xrightarrow{r \rightarrow 0} \delta_{mn} s_\ell(k_m r), \quad (29)$$

$$\phi_{mn}^{(\ell)}(r) \xrightarrow{r \rightarrow \infty} s_\ell(k_m r) A_{mn}^{(\ell)} + c_\ell(k_m r) B_{mn}^{(\ell)}. \quad (30)$$

The asymptotic $\phi_{mn}^{(\ell)}(r)$ at large r can be written in terms of the free solutions $e^{\pm ikr}$, namely

$$\begin{aligned} \phi_{mn}^{(\ell)}(r) &\xrightarrow{r \rightarrow \infty} \frac{i}{2} \left[(A_{mn}^{(\ell)} - iB_{mn}^{(\ell)}) e^{-i(k_m r - \ell\pi/2)} \right. \\ &\quad \left. - (A_{mn}^{(\ell)} + iB_{mn}^{(\ell)}) e^{+i(k_m r - \ell\pi/2)} \right], \end{aligned} \quad (31)$$

$$\equiv \frac{i^{\ell+1}}{2} \left[\mathcal{J}_{mn}^{(\ell)} e^{-ik_m r} - (-1)^\ell \mathcal{J}_{mn}^{(\ell)*} e^{+ik_m r} \right], \quad (32)$$

where, we define the Jost matrix element as

$$\mathcal{J}_{mn}^{(\ell)} \equiv A_{mn}^{(\ell)} - iB_{mn}^{(\ell)}. \quad (33)$$

or, in matrix form,

$$\overline{\phi}^{(\ell)}(r) \xrightarrow{r \rightarrow \infty} \frac{i^{\ell+1}}{2} [e^{-i\mathbf{K}r} \mathcal{J}_\ell - (-1)^\ell e^{i\mathbf{K}r} \mathcal{J}_\ell^*]. \quad (34)$$

Multiplying $\overline{\phi}^{(\ell)}$ by $i^\ell \mathcal{J}_\ell^{-1} C(\mathbf{K})$ on the right, we find by comparing with the physical solution given by Eq.(16),

$$\overline{\Psi}^{(\ell)} = i^\ell \overline{\phi}^{(\ell)} \mathcal{J}_\ell^{-1} C(\mathbf{K}), \quad (35)$$

with

$$\mathbf{S}^{(\ell)} = \mathbf{K}^{1/2} \mathcal{J}_\ell^* \mathcal{J}_\ell^{-1} \mathbf{K}^{-1/2} \quad (36)$$

If ℓ is not a good quantum number, for example due to interactions with external fields, the Jost-matrix can still be written in term of two matrices [33] as in Eq.(33)

$$\mathcal{J} \equiv \mathbf{A} - i\mathbf{B}. \quad (37)$$

and the matrix expression relating the S-matrix and the Jost-matrix is still valid

$$\mathbf{S} = \mathbf{K}^{1/2} \mathcal{J}^* \mathcal{J}^{-1} \mathbf{K}^{-1/2}. \quad (38)$$

The inverse of the Jost-matrix in \mathbf{S} is given by

$$\mathcal{J}^{-1} = \frac{1}{\det(\mathcal{J})} [\text{Cof}(\mathcal{J})]^T, \quad (39)$$

with $[\text{Cof}(\mathcal{J})]^T$ the transpose of the matrix of cofactors of \mathcal{J} and $\det(\mathcal{J})$ the determinant of \mathcal{J} . These expressions are particularly instructive to understand the effect a Near Threshold Resonance (NTR) on the scattering cross sections.

IV. NEAR THRESHOLD RESONANCES

We consider resonances occurring due to existence of a quasi-bound state in the entrance channel of a scattering system. We first look at few examples in benchmark chemical reactions, explain the energy scaling due to these near threshold resonances based on the properties of the Jost functions, and employ a three-open channel model to illustrate the effect for higher partial waves ℓ up to f -wave ($\ell = 3$). We end the discussion with the elastic case, where additional considerations on the range of the potential affect the validity of our results.

A. Benchmark reactions

In our previous work [26, 27], we have used two benchmark chemical reactions to investigate near threshold resonances in the ultracold temperature regime. In particular, we studied $\text{H}_2 + \text{Cl}$ and $\text{H}_2 + \text{F}$ reactions in the s -wave ($\ell = 0$) scattering regime, by varying the mass of H as suggested originally by [38], which changes the relative position of channels and bound and quasi-bound states,

allowing to theoretically tune resonances and scattering processes. This approach is similar to modifying the PES itself [39]. The results presented here were obtained using the ABC reactive scattering code of Manolopoulos and coworkers [40], which has been optimized for ultralow energies in previous studies of $\text{H}_2 + \text{D}$ [23], and $\text{H}_2 + \text{Cl}$ [26, 27],

The first case we discuss is $\text{H}_2 + \text{Cl}$ for s -wave scattering, for which the details of the calculations and mass scaling are given in [26, 27]. This system was recently investigated at ultralow temperatures [26, 27, 41]; we used the potential energy surface (PES) developed by Bian and Werner [42]. Fig. 1 shows the results for $\text{H}_2 + \text{Cl}$, with the left panels depicting the elastic σ_n^{elas} and total inelastic σ_n^{inel} cross sections for the initial channel n corresponding to $\text{H}_2(v = 1, j = 0) + \text{Cl}$ as a function of the mass of H, m , at a collision energy 1 nK. It shows sharp variations of the cross sections for specific values of m : the real mass of H (m_{H}) and D (m_{D}) are indicated by solid circles. The right panels illustrate the effect of near threshold resonances (NTRs) on cross sections for three values of m starting from m_{H} and getting closer to the resonance shown on the left panels. The cross sections are given as a function of the scattering energy $E = \hbar^2 k^2 / 2\mu$ defined from the threshold of the entrance channel.

As $k \rightarrow 0$, σ_n^{inel} reaches the Wigner's regime, scaling as k^{-1} for all three masses. For masses closer to the resonance, the scaling changes to k^{-3} at higher energies (still ultracold and described by $\ell = 0$ scattering only). This behavior appears to be universal; at higher energies (but still ultracold), σ_n^{inel} has the same value until it deviates from the universal NTR k^{-3} scaling to join the Wigner k^{-1} scaling at lower k . The elastic cross sections σ_n^{elas} is also shown for the same masses; the Wigner regimes constant cross section as $k \rightarrow 0$ changes to the expected k^{-2} scaling for m near a resonance.

Similar behaviors were found for $\text{H}_2 + \text{F}$ in the s -wave ($\ell = 0$) regime [27] using the PES developed by Stark and Werner [43]: this system has also been studied in the ultracold regime by [38, 44]. The origin of the NTR regime for $\ell = 0$ was investigated in our previous work, first as the result of the proximity of a pole of the S-matrix to the real positive k -axis [26], and then in terms of the Jost function [27]. More recently, we have explored other benchmark reactions involving hydrogen and its isotopes, namely $\text{H}_2 + \text{D}$ [25] and $\text{D}_2 + \text{H}$ [28] using the PES of [45], to probe the effect of the nuclear spin symmetry on the scattering processes. In particular, we identified a p -wave ($\ell = 1$) shape resonance in the $\text{H}_2(v = 1, j = 0) + \text{D}$ entrance channel for para- H_2 . The details of the calculations are given in [25]. In Fig. 2 (inset), we show the total inelastic cross section vs E for the real mass of H, with the leading contribution of s -wave ($\ell = 0$) scattering as $E \rightarrow 0$, the dominating contribution of the p -wave ($\ell = 1$) resonance near $E/k_B \sim 100$ mK, the smaller structure due to the d -wave ($\ell = 2$) near 5 K, and higher partial wave contributions at larger energies still.

The main plot of Fig. 2 depicts the p -wave contribu-

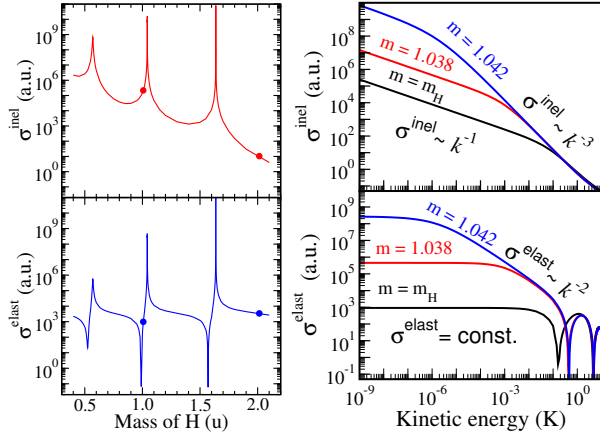


FIG. 1: Left panel: elastic and total inelastic cross sections vs. m (the mass of H, with circles stand for the true mass of H and D) for the entrance channel $\text{H}_2(v=1, j=0) + \text{Cl}$ at a collision energy $E/k_B = 1$ nK. Right panel: corresponding energy dependence of the inelastic (a) and elastic (b) cross sections for $m = 1.0078 \text{ u} = m_{\text{H}}$ (true mass), 1.038 u , and 1.042 u (blue).

tion only, for different value of m (mass of H). As m increases from the real mass of H (m_{H}), the position of the resonance shifts to lower energies and is accompanied by an increased magnitude until it disappears near $m \sim 1.018 \text{ u}$, at which point the van der Waals complex $\text{H}_2 \cdots \text{D}$ acquires a new bound state. As m increases further, the maximum in the cross section starts shifting to larger energies with a decreasing magnitude. We note that using Rydberg-dressed interactions between H_2 and D mimics the variation of the mass of H by changing the amount of Rydberg admixing in the colliding partners [24]. Fig. 2 clearly points to two k -scaling regimes on either side of the resonance, the expected k Wigner scaling as $k \rightarrow 0$, and a different k^{-3} NTR scaling at higher k . We also note that while the Wigner regime tends to different values (all with the k -dependence), the total inelastic cross section (p -wave) coalesces on a single curve in NTR regime, in a fashion similar to the s -wave NTR regime discussed above and shown in Fig. 1.

In the next section, we give a theoretical framework based on Jost functions, and generalize the treatment to any partial wave ℓ .

B. Jost function theoretical framework: inelastic processes

To explain the appearance of the NTR regime, we turn to the properties of the S -matrix. From Eq.(38), $\mathbf{S} = \mathbf{K}^{1/2} \mathcal{J}^* \mathcal{J}^{-1} \mathbf{K}^{-1/2}$, and Eq.(39), $\mathcal{J}^{-1} = [\text{Cof}(\mathcal{J})]^T / \det(\mathcal{J})$, we can rewrite the matrix element

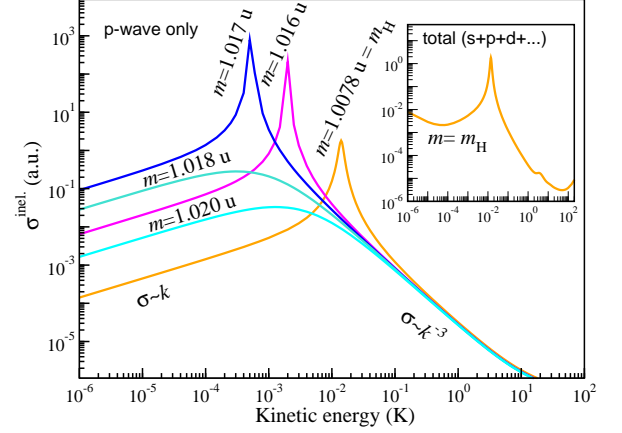


FIG. 2: The p -wave contribution for the total inelastic (including reaction) cross section for $\text{D} + \text{H}_2(v = 1, j = 0)$ for different values of m , as indicated. The inset shows the fully converged cross section, including partial waves $\ell = 0, 1, 2, 3, 4, \dots$

$S_{fi}^{(\ell)}$ for the partial cross section $\sigma_{f \leftarrow i}^{(\ell)}$ in Eq.(24) as

$$S_{fi} = \sqrt{\frac{k_f}{k_i}} \left(\mathcal{J}^* \frac{[\text{Cof}(\mathcal{J})]^T}{\det(\mathcal{J})} \right)_{fi} = \sqrt{\frac{k_f}{k_i}} \frac{\sum_j \mathcal{J}_{fj}^* C_{ij}}{\det(\mathcal{J})},$$

where we omit (ℓ) for simplicity, and $C_{ji} = \text{Cof}(\mathcal{J})_{ji}$ is the cofactor of \mathcal{J} . Adding and subtracting \mathcal{J}_{fj} in the sum, and with $\mathcal{J}_{fj}^* - \mathcal{J}_{fj} = 2iB_{fj}$, we have $\mathcal{J}_{fj}^* C_{ij} = \mathcal{J}_{fj} C_{ij} + 2iB_{fj} C_{ij}$, so that

$$\begin{aligned} \sum_j \mathcal{J}_{fj}^* C_{ij} &= \sum_j \mathcal{J}_{fj} C_{ij} + 2i \sum_j B_{fj} C_{ij} \\ &= \delta_{fi} \det(\mathcal{J}) + 2i \sum_j B_{fj} C_{ij}, \end{aligned} \quad (40)$$

where we use the properties of a determinant in term of cofactors. The matrix element S_{fi} is then

$$S_{fi} = \delta_{fi} + \sqrt{\frac{k_f}{k_i}} \frac{2i \sum_j B_{fj} C_{ij}}{\det(\mathcal{J})},$$

and the element T_{fi} of the T-matrix $\mathbf{T} = \mathbf{1} - \mathbf{S}$ simply becomes

$$T_{fi} = -2i \sqrt{\frac{k_f}{k_i}} \frac{\sum_j B_{fj} C_{ij}}{\det(\mathcal{J})}.$$

The partial cross section $\sigma_{f \leftarrow i}^{(\ell)}$ defined in Eq.(24) is

$$\sigma_{f \leftarrow i} = \frac{\pi}{k_i^2} |T_{fi}|^2 = \frac{4\pi k_f}{k_i^3} \frac{|\sum_j B_{fj} C_{ij}|^2}{|\det(\mathcal{J})|^2}. \quad (41)$$

The resonance being due to a quasi-bound state in the entrance channel i , we isolate its contribution and write

the determinant as

$$\det(\mathcal{J}) = \sum_n \mathcal{J}_{in} C_{in} = C_{ii}(\mathcal{J}_{ii} + \mathbf{j}_{ii}), \quad (42)$$

where

$$\mathbf{j}_{ii} \equiv \frac{1}{C_{ii}} \sum_{n \neq i} \mathcal{J}_{in} C_{in}. \quad (43)$$

The denominator $|\det(\mathcal{J})|^2$ of $\sigma_{f \leftarrow i}$ becomes

$$|\det(\mathcal{J})|^2 = |C_{ii}|^2 |D|^2, \quad \text{where } D \equiv \mathcal{J}_{ii} + \mathbf{j}_{ii}. \quad (44)$$

As the resonance is in the entrance channel i , the cofactor C_{ii} includes all but the entrance channel and is a well-behaved function almost independent of k_i as $k_i \rightarrow 0$ [27]. The effect of the resonance is accounted for in D (mostly via the \mathcal{J}_{ii} contribution since \mathbf{j}_{ii} includes all other channels). For clarity, we label the entrance channel defining the threshold for the scattering energy by $i = 1$, and simply adopt the notation $k_i = k_1$ and $\ell_i = \ell_1$, so that

$$\sigma_{f \leftarrow 1} = \frac{4\pi k_f}{k_1^3} \frac{|\sum_j B_{fj} C_{1j}|^2}{|C_{11}|^2 |D|^2}. \quad (45)$$

To understand the behavior of $\sigma_{f \leftarrow 1}$ at small k_1 , we examine the k_1 -dependence of $B_{mn}(k_1)$ and $C_{mn}(k_1)$ starting from that of $A_{mn}(k_1)$ and $B_{mn}(k_1)$ extracted from Eqs.(29) and (30). If none of the index include the initial channel, we find

$$\left. \begin{array}{l} m \neq 1 \\ n \neq 1 \end{array} \right\} \Rightarrow \left\{ \begin{array}{l} A_{mn} = A_{mn}^{(0)} + A_{mn}^{(2)} k_1^2 + \dots, \\ B_{mn} = B_{mn}^{(0)} + B_{mn}^{(2)} k_1^2 + \dots, \end{array} \right. \quad (46)$$

where $A_{mn}^{(s)}$ and $B_{mn}^{(s)}$ for various s are constants. If both m and n are equal to one, we have

$$\left. \begin{array}{l} m = 1 \\ n = 1 \end{array} \right\} \Rightarrow \left\{ \begin{array}{l} A_{11} = A_{11}^{(0)} + A_{11}^{(2)} k_1^2 + \dots, \\ B_{11} = k_1^{2\ell_1+1} (B_{11}^{(0)} + B_{11}^{(2)} k_1^2 + \dots), \end{array} \right. \quad (47)$$

while if only one index is equal to one, we find

$$\left. \begin{array}{l} m \neq 1 \\ n = 1 \end{array} \right\} \Rightarrow \left\{ \begin{array}{l} A_{m1} = k_1^{\ell_1+1} (A_{m1}^{(0)} + A_{m1}^{(2)} k_1^2 + \dots), \\ B_{m1} = k_1^{\ell_1+1} (B_{m1}^{(0)} + B_{m1}^{(2)} k_1^2 + \dots), \end{array} \right. \quad (48)$$

and

$$\left. \begin{array}{l} m = 1 \\ n \neq 1 \end{array} \right\} \Rightarrow \left\{ \begin{array}{l} A_{1n} = k_1^{-\ell_1-1} (A_{1n}^{(0)} + A_{1n}^{(2)} k_1^2 + \dots), \\ B_{1n} = k_1^{\ell_1} (B_{1n}^{(0)} + B_{1n}^{(2)} k_1^2 + \dots). \end{array} \right. \quad (49)$$

From these, we get (with $f \neq 1$)

$$\left. \begin{array}{l} B_{11} \sim k_1^{2\ell_1+1} \\ B_{f1} \sim k_1^{\ell_1+1} \\ B_{1j \neq 1} \sim k_1^{\ell_1} \\ B_{fj \neq 1} \sim \text{const.} \end{array} \right\}, \text{ and } \left. \begin{array}{l} C_{11} \sim C_{11}^{(0)} = \text{const.} \\ C_{1j \neq 1} \sim C_{1j \neq 1}^{(0)} k_1^{\ell_1+1} \end{array} \right\}, \quad (50)$$

where both $C_{11}^{(0)}$ and $C_{1j \neq 1}^{(0)}$ are complex constant. For inelastic processes ($f \neq 1$), these give $\sum_j B_{fj} C_{1j} \sim k_1^{\ell_1+1}$, so that, together with k_f reaching a finite value as $k_1 \rightarrow 0$, we obtain

$$\sigma_{f \leftarrow 1}^{\text{inel}} \sim \frac{k_f}{k_1^3} \frac{\text{const.} k_1^{2\ell_1+2}}{|D(k_1)|^2} \sim \frac{k_1^{2\ell_1-1}}{|D(k_1)|^2}. \quad (51)$$

The elastic case with $f = 1$ is treated separately in Section IV D. The exact behavior of the cross sections will be dictated by that of $D(k_1)$.

We focus our attention on D , using $k \equiv k_1$ and $\ell \equiv \ell_1$ for clarity. From its definition in Eq.(44) together with $\mathcal{J}_{11} = A_{11} - iB_{11}$, we get

$$D(k) = A_{11} - iB_{11} + \mathbf{j}_{11},$$

where $\mathbf{j}_{11} = C_{11}^{-1} \sum_{n \neq 1} (A_{1n} - iB_{1n}) C_{1n}$ from Eq.(43). Using the leading terms in Eq.(49) together with $C_{11} \sim C_{11}^{(0)} = \text{const.}$ and $C_{1n \neq 1} \sim C_{1n \neq 1}^{(0)} k^{\ell+1}$ given in Eq.(50). we write

$$\begin{aligned} \mathbf{j}_{11} &= \frac{1}{C_{11}^{(0)}} \sum_{n \neq 1} \left[k^{-\ell-1} (A_{1n}^{(0)} + k^2 A_{1n}^{(2)} + \dots) \right. \\ &\quad \left. - i k^\ell (B_{1n}^{(0)} + k^2 B_{1n}^{(2)} + \dots) \right] C_{1n}^{(0)} k^{\ell+1}, \\ &= \sum_{n \neq 1} \frac{C_{1n}^{(0)}}{C_{11}^{(0)}} \left[(A_{1n}^{(0)} + k^2 A_{1n}^{(2)} + \dots) \right. \\ &\quad \left. - i k^{2\ell+1} (B_{1n}^{(0)} + k^2 B_{1n}^{(2)} + \dots) \right], \\ &\equiv \mathbf{j}_0 + \mathbf{j}_2 k^2 + \dots - i k^{2\ell+1} (\mathbf{g}_0 + \mathbf{g}_2 k^2 + \dots). \end{aligned} \quad (52)$$

Here, the complex numbers $\mathbf{j}_i \equiv \sum_{n \neq 1} A_{1n}^{(i)} C_{1n}^{(0)} / C_{11}^{(0)}$ and $\mathbf{g}_i \equiv \sum_{n \neq 1} B_{1n}^{(i)} C_{1n}^{(0)} / C_{11}^{(0)}$ have small magnitudes. Together with Eq.(47), we obtain

$$\begin{aligned} D(k) &= [(A_0 + \mathbf{j}_0) + (A_2 + \mathbf{j}_2) k^2 + \dots] \\ &\quad - i k^{2\ell+1} [(B_0 + \mathbf{g}_0) + (B_2 + \mathbf{g}_2) k^2 + \dots], \end{aligned} \quad (53)$$

where we use the simpler notation $A_i \equiv A_{11}^{(i)}$ and $B_i \equiv B_{11}^{(i)}$. The exact form of $D(k)$ depends on the value of ℓ , and for this reason, we consider $\ell = 0$ and $\ell \geq 1$ separately.

• $\ell = 0$: in this case, we have

$$\begin{aligned} D(k) &= [(A_0 + \mathbf{j}_0) + (A_2 + \mathbf{j}_2) k^2 + \dots] \\ &\quad - i k [(B_0 + \mathbf{g}_0) + (B_2 + \mathbf{g}_2) k^2 + \dots], \\ &= D_0 + D_1 k + D_2 k^2 + D_3 k^3 + \dots \end{aligned}$$

where $D_0 = A_0 + \mathbf{j}_0$, $D_1 = -i(B_0 + \mathbf{g}_0)$, $D_2 = (A_2 + \mathbf{j}_2)$, $D_3 = -i(B_2 + \mathbf{g}_2)$, and so on. The expansion of $|D|^2$ takes the form

$$|D(k)|^2 \simeq \Delta_0 + \Delta_1 k + \Delta_2 k^2 + \dots, \quad (54)$$

with $\Delta_0 = |D_0|^2$, $\Delta_1 = D_0^* D_1 + D_0 D_1^*$, $\Delta_2 = |D_1|^2 + D_0^* D_2 + D_0 D_2^*$, etc. The denominator $|D|^2$ will exhibit

the Wigner or NTR scaling depending on the magnitude of A_0 . If A_0 is dominant, then D_0 is also sizable and Δ_0 is the leading term in Eq.(54) for small k . However, if A_0 itself small, and since the magnitude of j_0 is also small, there is a range of k where Δ_0 is not the dominant contribution, and since Δ_1 is also proportional to D_0 , the next leading term is $\Delta_2 \approx |D_1|^2$ (since both $D_0 D_2^*$ and $D_0^* D_2$ must also be small). This condition gives the NTR scaling for a given range of k . To understand the Wigner and NTR regimes, Δ_1 can be omitted in Eq.(54) since it plays a role only in the transition between the two regimes. Combining these results with Eq.(51) gives (with $\ell = 0$)

$$\sigma_{\ell=0}^{\text{inel.}} \equiv \sigma_{f \leftarrow 1}^{\text{inel.}(\ell=0)} \sim \frac{k^{-1}}{\Delta_0 + k^2 \Delta_2}. \quad (55)$$

From Eqs.(45) and (51), we note that this k -scaling is the same for any exit channel $f \neq 1$, although each channel has its specific magnitude. The appearance of the NTR scaling depends of the relative strength of Δ_0 and Δ_2 . From Eq.(55), we have for inelastic processes

$$\sigma_{\ell=0}^{\text{inel.}} \sim \begin{cases} k^{-1}, & \text{Wigner: } k \ll \sqrt{|\Delta_0/\Delta_2|}, \\ k^{-3}, & \text{NTR: } k \gg \sqrt{|\Delta_0/\Delta_2|}, \end{cases} \quad (56)$$

• $\ell \neq 0$: we first consider $\ell = 1$. From Eq.(53), we have

$$\begin{aligned} D(k) &= [(A_0 + j_0) + (A_2 + j_2)k^2 + \dots] \\ &\quad - ik^3 [(B_0 + \mathbf{g}_0) + (B_2 + \mathbf{g}_2)k^2 + \dots], \\ &= D_0 + D_2 k^2 + \tilde{D}_3 k^3 + D_4 k^4 + \dots \end{aligned}$$

where $D_0 = A_0 + j_0$ and $D_2 = (A_2 + j_2)$ as before, $D_4 = A_4 + j_4$, and $\tilde{D}_3 = -i(B_0 + \mathbf{g}_0)$ (same as D_1 in the $\ell = 0$ case), and so on. The expansion of $|D|^2$ becomes

$$|D(k)|^2 \simeq \Delta_0 + \Delta_2 k^2 + \Delta_3 k^3 + \Delta_4 k^4 + \dots, \quad (57)$$

with $\Delta_0 = |D_0|^2$, $\Delta_2 = D_0^* D_2 + D_0 D_2^*$, $\Delta_3 = D_0^* \tilde{D}_3 + D_0 \tilde{D}_3^*$, $\Delta_4 = |D_2|^2 + D_0^* D_4 + D_0 D_4^*$, etc. Again, when A_0 is dominant, D_0 is also sizable, and Δ_0 is the leading term in Eq.(57) for small k , corresponding to the Wigner regime. If A_0 (and j_0) is small, then D_0 is small, and there is a range of k for which Δ_0 , Δ_2 and Δ_3 are small compared to $\Delta_4 \approx |D_2|^2$. As in the $\ell = 0$ case, Δ_2 and Δ_3 play a role in the transition between the Wigner (with Δ_0 dominant) and NTR (with Δ_4 dominant) regimes, and can be omitted to describe the two regimes. We write

$$|D(k)|^2 \approx \Delta_0 + \Delta_4 k^4 + \dots. \quad (58)$$

Similarly, for $\ell = 2$, Eq.(53) gives

$$\begin{aligned} D(k) &= [(A_0 + j_0) + (A_2 + j_2)k^2 + \dots] \\ &\quad - ik^5 [(B_0 + \mathbf{g}_0) + (B_2 + \mathbf{g}_2)k^2 + \dots], \\ &= D_0 + D_2 k^2 + D_4 k^4 + \tilde{D}_5 k^5 \dots \end{aligned}$$

where, D_0 , D_2 , and D_4 are given above, and $\tilde{D}_5 = -i(B_0 + \mathbf{g}_0)$ (same as D_1 in the $\ell = 0$ case), and so on. The expansion of $|D|^2$ becomes

$$|D(k)|^2 \simeq \Delta_0 + \Delta_2 k^2 + \Delta_4 k^4 + \dots, \quad (59)$$

with Δ_0 , Δ_2 , Δ_4 are the same as for $\ell = 1$. There is no k^3 term, which holds for $\ell > 2$ in general. Again, for a sizable A_0 , Δ_0 is the leading term in Eq.(59) at small k , and for small A_0 , there is a range of k for which $\Delta_4 \approx |D_2|^2$ is the leading term: Δ_2 plays a role in the transition between the Wigner (with Δ_0 dominant) and NTR (with Δ_4 dominant) regimes, and is omitted. The same expression for $|D|^2$ can therefore be used for $\ell = 1$ and $\ell \geq 2$, namely

$$|D(k)|^2 \approx \Delta_0 + \Delta_4 k^4 + \dots. \quad (60)$$

Combining this result with Eq.(51), we get

$$\sigma_{\ell \neq 0}^{\text{inel.}} \equiv \sigma_{f \leftarrow 1}^{\text{inel.}(\ell \neq 0)} \sim \frac{k^{2\ell-1}}{\Delta_0 + k^4 \Delta_4}. \quad (61)$$

As in the $\ell = 0$ case in Eq.(55), this k -scaling is the same for any exit channel $f \neq 1$, each channel having its specific magnitude. Eq.(61) shows that the appearance of the NTR scaling depends of the relative strength of Δ_0 and Δ_4 .

$$\sigma_{\ell \neq 0}^{\text{inel.}} \sim \begin{cases} k^{2\ell-1}, & \text{Wigner: } k \ll |\Delta_0/\Delta_4|^{1/4}, \\ k^{2\ell-5}, & \text{NTR: } k \gg |\Delta_0/\Delta_4|^{1/4}, \end{cases} \quad (62)$$

We note that for $\ell = 1$, the scaling leads to a k^{-3} NTR scaling for inelastic processes, as for $\ell = 0$. This is illustrated for the benchmark system $\text{H}_2 + \text{D}$ in Fig. 2.

In general, the NTR regime appears when Δ_0 is small when compared to Δ_2 (for $\ell = 0$) or Δ_4 (for $\ell \geq 1$). The transition between the Wigner and NTR regimes takes place around $k = \sqrt{\Delta_0/\Delta_2}$ for $\ell = 0$ or around $k = \sqrt{\Delta_0/\Delta_4}$ for $\ell > 0$. In [27], we explored this transition in $\text{H}_2 + \text{Cl}$ for $\ell = 0$ for the three resonances shown in Fig. 1 by plotting the reaction probability $P = 1 - |S_{ii}|^2$, a smooth function, also showing the effect of the reactivity (or background cross section away from the resonance: see [27] for more details).

C. Simple model

Since resonances usually become narrower with higher ℓ , and occur at higher scattering energies, the computational cost for benchmark systems containing H_2 quickly become prohibitive. Instead, we illustrate the effect of NTRs on cross sections using a simpler model incorporating the key ingredients while allowing for easy tuning of the resonances for each partial wave ℓ .

Fig. 3 depicts the model: it consists of three open channels with an attractive r^{-6} potential tail and a short-range hard wall. The position r_0 of the hard wall is

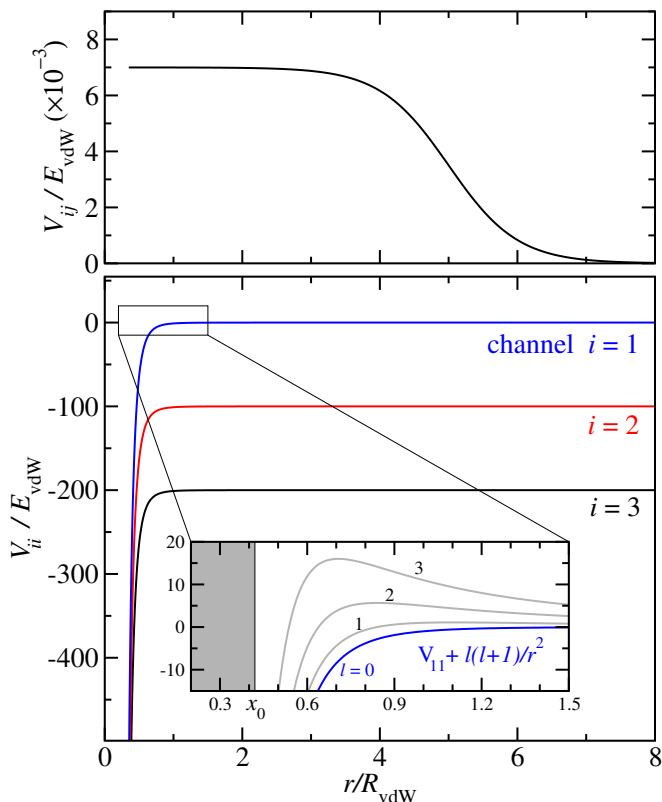


FIG. 3: Upper panel: coupling potential, see Eq. (64), used in our three-channel model. Lower panel: diagonal potentials, see Eq. (63). The inset shows the effective potential in the entrance channel for $\ell \leq 3$.

shifted slightly for each partial wave as to bring a resonance in the entrance channel $i = 1$. The diagonal potentials V_{ii} are identical for each channel i , each with their own threshold E_i . To simplify notations, we use van der Waals units R_{vdW} for the length and $E_{\text{vdW}} = \hbar^2/2\mu R_{\text{vdW}}^2$ for energy, where μ is the reduced mass of the scattering partners. For an attractive power-law tail $V(r) \sim -C_\alpha r^{-\alpha}$, the van der Waals length scale is $R_{\text{vdW}} = (2\mu C_\alpha/\hbar^2)^{\frac{1}{\alpha-2}}$. The off-diagonal couplings V_{ij} are taken to be identical and short-range. Defining $x \equiv r/R_{\text{vdW}}$, the diagonal and off-diagonal potentials have the form

$$V_{nn}(r) = \begin{cases} +\infty & , \text{ for } r \leq r_0, \\ -\frac{E_{\text{vdW}}}{x^6} + E_i & , \text{ for } r > r_0 \end{cases}, \quad (63)$$

$$V_{ij} = \frac{0.007E_{\text{vdW}}}{1 + \exp[2(x-5)]}. \quad (64)$$

The energy threshold for each channel i and the values of r_0 bringing a near threshold resonance in the entrance channel for a given partial wave ℓ are respectively

$$\frac{E_i}{E_{\text{vdW}}} = \begin{cases} 0 & , \text{ for channel 1} \\ -100 & , \text{ for channel 2} \\ -200 & , \text{ for channel 3} \end{cases}, \quad (65)$$

and

$$\frac{r_0}{R_{\text{vdW}}} = \begin{cases} 0.42402677 & , \text{ for } \ell = 0 \\ 0.37845091 & , \text{ for } \ell = 1 \\ 0.34646173 & , \text{ for } \ell = 2 \\ 0.32219300 & , \text{ for } \ell = 3 \end{cases}. \quad (66)$$

For simplicity sake, only the entrance channel $i = 1$ contains the centrifugal term $\ell(\ell+1)/x^2$.

We compute the partial cross sections $\sigma_{f \leftarrow 1}^{\text{inel},(\ell)}$ for each ℓ and for the final channel being 2 or 3. The results are shown in Fig. 4, where the axes of each panel have different ranges due to the changing resonance width and position. They demonstrate that for both final channels, the inelastic partial cross section follows the k -scaling given by Eq.(62) for $\ell = 0$ and Eq.(62) for $\ell \geq 1$. More specifically, it verifies that the NTR regime scaling multiplies the Wigner regime by k^{-2} for $\ell = 0$, and by k^{-4} otherwise. Since the resonance is in the entrance channel, the partial inelastic cross section into the two remaining final channels are basically identical within an overall constant.

D. Elastic processes

In the elastic case, the range of the interaction potential may play an important role in the k -scaling of the cross section. We therefore consider short-range and long-range (actually power-law type) interactions separately.

1. Short-range

The previous treatment applies to this case (*e.g.*, for interaction with long-range exponential tail like the Morse-type potential). For $f = 1$, and replacing $k_f = k_1 \equiv k$ in Eq.(45), and using the results of Eq.(50), we have $\sum_j B_{1j}C_{1j} \sim k^{2\ell+1}$, so that

$$\sigma_{1 \leftarrow 1}^{\text{elas}} \sim \frac{k \text{ const.} k^{4\ell+2}}{k^3 |D(k)|^2} \sim \frac{k^{4\ell}}{|D(k)|^2}. \quad (67)$$

The previous results for $|D(k)|^2$ apply here as well, and we obtain for $\ell = 0$

$$\sigma_{\ell=0}^{\text{elas}} \sim \frac{k^0}{\Delta_0 + k^2 \Delta_2}, \quad (68)$$

leading to

$$\sigma_{\ell=0}^{\text{elast}} \sim \begin{cases} k^0 & , \text{ Wigner: } k \ll \sqrt{|\Delta_0/\Delta_2|}, \\ k^{-2} & , \text{ NTR: } k \gg \sqrt{|\Delta_0/\Delta_2|}. \end{cases} \quad (69)$$

For $\ell \geq 1$, we get

$$\sigma_{\ell \neq 0}^{\text{elas}} \sim \frac{k^{4\ell}}{\Delta_0 + k^4 \Delta_4}, \quad (70)$$

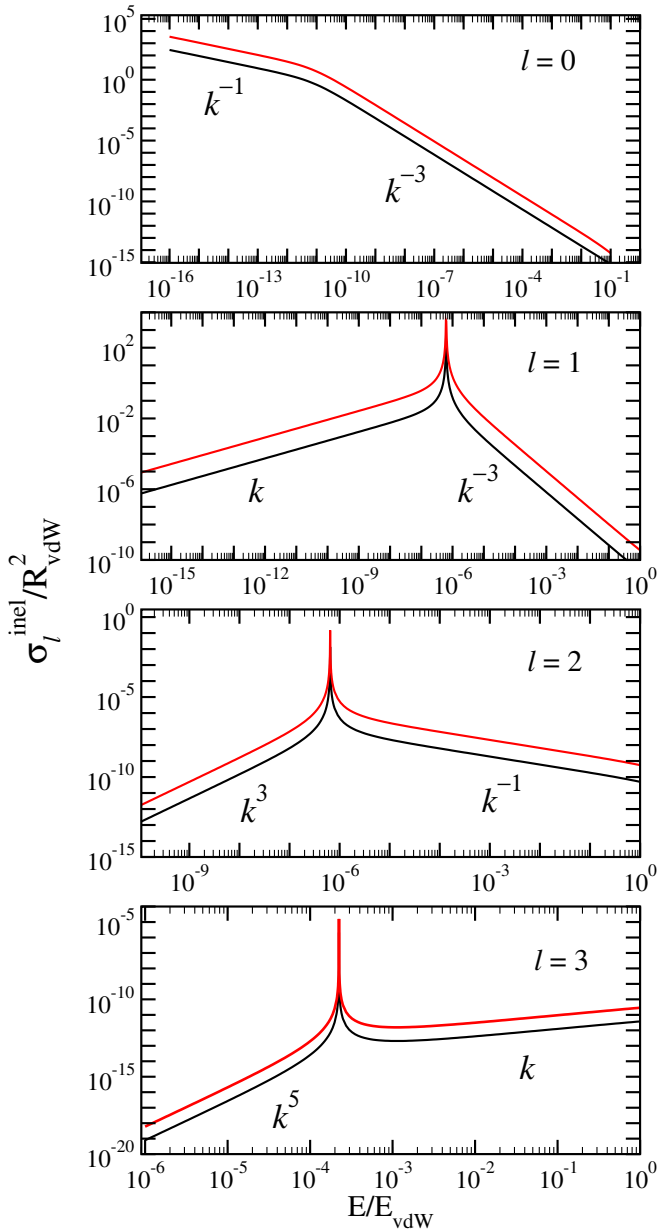


FIG. 4: Simple model: individual partial inelastic cross sections $\sigma_{f \leftarrow i}^{\text{inel},(\ell)}$ for $\ell = 0, \dots, 3$ as a function of the scattering energy E . Both E and σ are given in scaled van der Waals units E_{vdW} and R_{vdW} , respectively, with different range for the cross section for each ℓ . Red and black curves correspond to the different final channels $i = 1 \rightarrow f = 2$ and $i = 1 \rightarrow f = 3$, respectively.

leading to

$$\sigma_{\ell \neq 0}^{\text{elast}} \sim \begin{cases} k^{4\ell} & , \text{Wigner: } k \ll |\Delta_0/\Delta_4|^{1/4}, \\ k^{4\ell-4} & , \text{NTR: } k \gg |\Delta_0/\Delta_4|^{1/4}. \end{cases} \quad (71)$$

We note that the NTR regime scales as k^0 for $\ell = 1$. Fig. 5 shows the elastic cross section for the model of the previous section, *i.e.* a long-range tail of the form $-C_6/r^6$. For both $\ell = 0$ and 1, we observe the expected

scalings for the Wigner and NTR regimes. However, the k -scaling for higher ℓ values does not seem to follow Eq.(71); for $\ell = 3$, below and above the resonance, the scaling follows k^6 instead of the expected k^{12} (Wigner) and k^8 (NTR) scalings. This is due to the power-law long-range tail of the interaction potential. As we will see below, even for $\ell = 2$, the k -scaling shown in Fig. 5, though seemingly agreeing with the short-range scaling k^8 (Wigner) and k^4 (NTR) given by Eq.(71), it is actually not following the appropriate Wigner scaling regime. To understand these details, we consider the effect of the power-law tail on the elastic cross section.

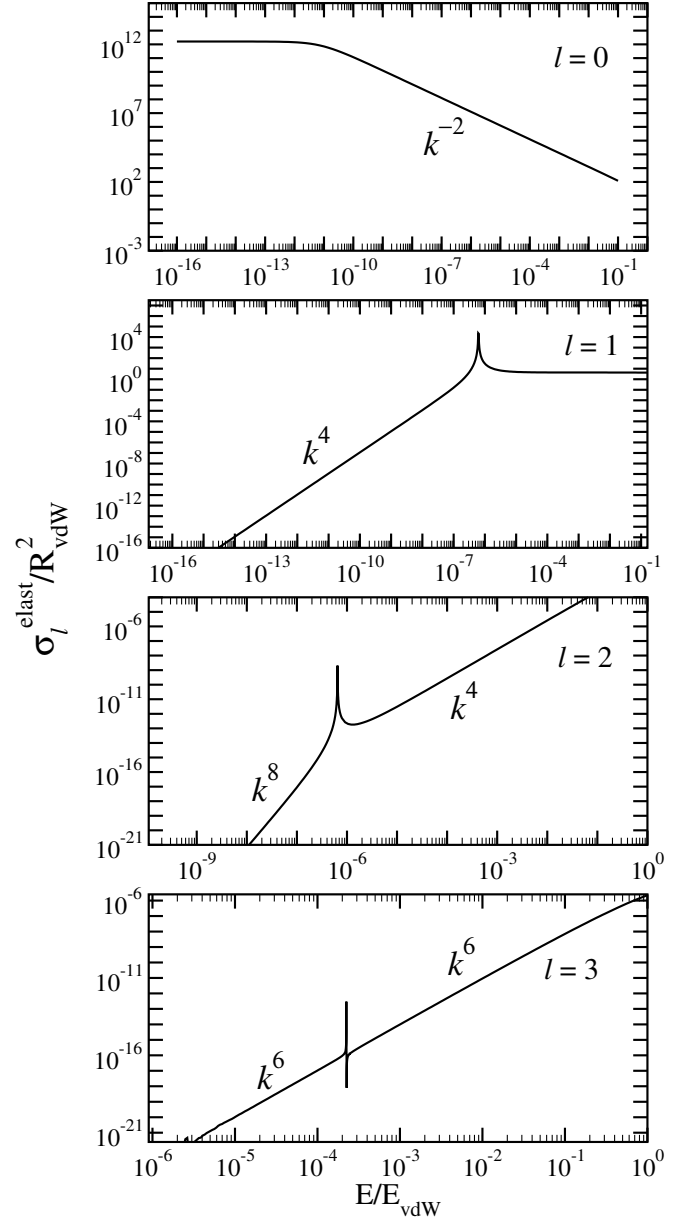


FIG. 5: Same as Fig. 4 for the elastic cross section; see text for discussion.

2. Power-law tail

While the threshold behavior (including both NTR and Wigner regimes) of the inelastic cross sections is unaffected by the long-range nature of the diagonal potential in the entrance channel, the elastic cross section at low energy can be altered significantly by the long-range tail of $V_{11}(r)$. This can be understood in terms of the single-channel Jost function, $\mathcal{J} = A - iB$, corresponding to the entrance channel ($n = 1$). Using $S = \mathcal{J}^* \mathcal{J}^{-1}$, the partial single-channel elastic cross section (for a given ℓ) is simply

$$\sigma_\ell^{\text{elas}} = \frac{4\pi}{k^2} |1 - S_\ell(k)|^2 = \frac{4\pi}{k^2} \frac{B^2(k)}{A^2(k) + B^2(k)}, \quad (72)$$

where we omit the subscript ℓ for A_ℓ and B_ℓ for clarity. According to Willner and Gianturco [46], the k -dependence of the single-channel Jost function for a potential which behaves asymptotically ($r \rightarrow \infty$) as an inverse power, $V(r) \approx r^{-\alpha}$, takes the form

$$\left. \begin{aligned} A(k) &= \tilde{A}(k)L^{AA}(k) + \tilde{B}(k)L^{AB}(k), \\ B(k) &= \tilde{B}(k)L^{BB}(k) + \tilde{A}(k)L^{BA}(k), \end{aligned} \right\} \quad (73)$$

where $\tilde{A}(k)$ and $\tilde{B}(k)$ are analytic functions,

$$\left. \begin{aligned} \tilde{A}(k) &= A_0 + A_2 k^2 + \dots, \\ \tilde{B}(k) &= k^{2\ell+1}(B_0 + B_2 k^2 + \dots), \end{aligned} \right\} \quad (74)$$

while the functions $L(k)$ contain the effect of the long-range tail, and can be expanded as power series (possibly including log-terms) [46],

$$\left. \begin{aligned} L^{AA}(k) &= 1 + a(C_\alpha k^{\alpha-2}) + a'(C_\alpha k^{\alpha-2})^2 + \dots, \\ L^{BB}(k) &= 1 + b(C_\alpha k^{\alpha-2}) + b'(C_\alpha k^{\alpha-2})^2 + \dots, \\ L^{AB}(k) &= c(C_\alpha k^{\alpha-2}) + c'(C_\alpha k^{\alpha-2})^2 + \dots, \\ L^{BA}(k) &= d(C_\alpha k^{\alpha-2}) + d'(C_\alpha k^{\alpha-2})^2 + \dots, \end{aligned} \right\} \quad (75)$$

where $a, a', b, b', c, c', d, d', \dots$, are constants.

In general, one must keep both ‘‘normal’’ and ‘‘mixed/cross’’ terms when truncating the low- k expansions for A and B , giving

$$\left. \begin{aligned} A(k) &\approx A_0 + A_2 k^2 + B_0 c C_\alpha k^{2\ell+\alpha-1} + \dots, \\ B(k) &\approx (A_0 + A_2 k^2) d C_\alpha k^{\alpha-2} + B_0 k^{2\ell+1} + \dots \end{aligned} \right\} \quad (76)$$

Thus, unlike the short-range case, the k -dependence of the Jost function for a long-range potential is considerably more complex. In particular, for $\ell \geq \frac{1}{2}(\alpha - 3)$, the dominant term for $B(k)$ at low- k will no longer be $B_0 k^{2\ell+1}$, but $A_0 d C_\alpha k^{\alpha-2}$ instead. Consequently, when A_0 is vanishingly small (NTR case), both $A(k)$ and $B(k)$ can lose their dominant term simultaneously. This is particularly important for the elastic cross section in Eq.(72), since it contains $B(k)$ in the numerator.

3. $\alpha = 6$

Let us explore the specific case $\alpha = 6$ corresponding to our model and most interactions for neutral ground state scattering partners (without permanent dipole or quadrupole moments). In that case, the critical (transition) value for the angular momentum is $\ell_* = \frac{\alpha-3}{2} = \frac{3}{2}$. Thus, for s -wave and p -wave, the leading k powers in A and B are the same as the short-range case, and so is the low- k behavior of the elastic cross section, while for d -wave and higher ($\ell \geq \frac{3}{2}$) we expect new types of behavior.

Partial wave $\ell = 2$

According to Eq.(76), with $\alpha = 6$ and $\ell = 2$, we have

$$\begin{aligned} A(k) &\approx A_0 + A_2 k^2 + B_0 c C_6 k^5 + \dots, \\ B(k) &\approx (A_0 + A_2 k^2) d C_6 k^4 + B_0 k^5 + \dots \end{aligned}$$

In the absence of NTR, A_0 is sizable, and $A(k) \sim A_0$ while $B(k) \sim A_0 d C_6 k^4 \propto k^4$, so that the Wigner regime behavior of the elastic cross section should be

$$\sigma_{\ell=2}^{\text{elas}} = \frac{4\pi}{k^2} \frac{B^2}{A^2 + B^2} \propto k^6, \text{ bare/true Wigner.} \quad (77)$$

However, when a shape resonance is very close to the threshold, A_0 becomes vanishingly small, and the Wigner regime practically disappears into the very-very-deep ultracold. In Fig. 5, it would be visible at much lower energies (not shown).

Indeed, for $\ell = 2$, $B(k) \approx A_0 d C_6 k^4 + B_0 k^5$, and the competition between the leading order term ($A_0 d C_6 k^4$) and the next order term ($B_0 k^5$) leads to a transition at around $k_B \sim |A_0 d C_6 / B_0|$. However, the denominator $A^2 + B^2$ is dominated by $A(k) \approx A_0 + A_2 k^2$ at small k , giving to a transition between the leading term (A_0) and the next order term ($A_2 k^2$) at $k_A \sim |A_0 / A_2|^{1/2}$. For the NTR condition, A_0 becomes small, and although both k_B and k_A vanish with A_0 , k_B vanishes much faster than k_A , and a new (intermediate) regime appears. This new regime ($k_B < k < k_A$) can be regarded as the (effective) Wigner regime, because the (bare/true) Wigner regime itself ($k < k_B$) is lost in the deep ultracold.

Within the new (effective Wigner) regime, the A_0 term is negligible in the numerator so that $B^2(k) \sim B_0^2 k^{10}$, but it is still dominant in the denominator $A^2(k)$, and we have:

$$\sigma_{\ell=2}^{\text{elas}} \sim \frac{4\pi}{k^2} \frac{B_0^2 k^{10}}{A_0^2} \sim k^8, \text{ effective Wigner regime.} \quad (78)$$

As mentioned above, the $\ell = 2$ k -scaling in Fig. 5 shows the effective Wigner regime k^8 scaling, the bare/true Wigner k^6 regime appearing at much lower energies (not shown).

Partial waves $\ell = 3$ and higher

For $\ell \geq 3$, the leading orders for A and B according to Eq.(76) are $A(k) \approx A_0 + A_2k^2$, and $B(k) \approx (A_0 + A_2k^2)dC_6k^4$. The B_0 terms can be neglected because they are of higher order (k^{11} in A and k^7 in B for $\ell = 3$). Thus, except in the immediate vicinity of the very narrow shape resonance, we have:

$$\sigma_{\ell \geq 3}^{\text{elas}} \sim \frac{4\pi [(A_0 + A_2k^2)dC_6k^4]^2}{k^2 (A_0 + A_2k^2)^2} \propto k^6. \quad (79)$$

Hence, there is only one power law for both Wigner and NTR regimes (with a narrow spike/resonance in the middle), as depicted in Fig. 5.

V. CONCLUSION

In this paper, we investigated the effect of near threshold resonances (NTRs) on both the elastic and inelastic cross sections for given partial waves ℓ at low scattering energies. In particular, we considered benchmark reactions involving molecular hydrogen, $\text{H}_2 + \text{Cl}$ (for s -wave) and $\text{H}_2 + \text{D}$ (for p -wave). The later possesses resonant features that are reachable experimentally. For higher partial waves, we used a three open channel model incorporating the key ingredients relevant to NTRs. The interaction potentials in all those cases have a r^{-6} long-range tail. We numerically found that the inelastic cross sections follows two k -scaling laws, namely $\sigma_{\ell=0}^{\text{inel.}} \sim k^{-1}$ (Wigner) and k^{-3} (NTR), and $\sigma_{\ell \neq 0}^{\text{inel.}} \sim k^{2\ell-1}$ (Wigner) and $k^{2\ell-5}$ (NTR). These scalings follow those obtained by analyzing the analytical behavior of the inelastic cross section for short-range interactions, based on Jost functions. This is to be expected, since inelastic scattering processes are due to short-range couplings overtaking the long-range tail of the diagonal term of the interaction matrix.

The case of elastic scattering is slightly different. The results for short-range interactions were found to be $\sigma_{\ell=0}^{\text{elas}} \sim k^0$ (Wigner) and k^{-2} (NTR), and $\sigma_{\ell \neq 0}^{\text{elas.}} \sim k^{4\ell}$ (Wigner) and $k^{4\ell-4}$ (NTR). However, the long-range tail of the interaction affects some partial waves. In the r^{-6} case considered here, we found that $\ell = 0$ and 1 follow the short-range results, but for $\ell \geq 2$, the power-law tail modifies those scalings. For $\ell = 2$, the true Wigner regime scales like k^6 (instead of the short-range k^8), while the NTR regime scales like the expected k^4 ; however, we witnessed the appearance of an effective Wigner regime scaling as k^8 between those two regimes. For $\ell > 2$, the cross section follows a k^6 scaling which does not agree with either the Wigner or the NTR scalings for short-range potentials. These results hint at a vanishingly relevant effect of a resonance on the elastic cross section with increasing ℓ ; beside a sharp and narrow feature at resonance, the k -scaling is “monotonic”.

Understanding the effect of near threshold resonances on scattering processes is important to help understanding but also predict the behavior of ultracold systems. The different k -scaling of elastic and inelastic cross sections can help guiding experimental efforts at cooling ultracold molecular samples.

Again, understanding the behavior of ultracold samples, atomic or molecular, requires understanding the role played by resonances, such as NTRs. They dictate the behavior of ultracold systems, and can be used to manipulate and control processes in these systems.

Acknowledgments

This work was partially supported by the MURI US Army Research Office Grant No. W911NF-14-1-0378 (IS) and by the US Army Research Office, Chemistry Division, Grant No. W911NF-13-1-0213 (DS, RC).

-
- [1] C. D. Gay, P. C. Stancil, S. Lepp, and A. Dalgarno, *Astrophys. J.* **737**, 44 (2011), URL <http://stacks.iop.org/0004-637X/737/i=1/a=44>.
 - [2] D. Galli and F. Palla, *Planet. Space Sci.* **50**, 1197 (2002), ISSN 0032-0633, Special issue on Deuterium in the Universe, URL <http://www.sciencedirect.com/science/article/pii/S0032063302000831>.
 - [3] R. Côté and A. Dalgarno, *Chem. Phys. Lett.* **279**, 50 (1997), ISSN 0009-2614.
 - [4] R. Côté and A. Dalgarno, *J. Mol. Spectr.* **195**, 236 (1999), ISSN 0022-2852, URL <http://www.sciencedirect.com/science/article/pii/S0022285299978372>.
 - [5] A. Fioretti, D. Comparat, A. Crubellier, O. Dulieu, F. Masnou-Seeuws, and P. Pillet, *Phys. Rev. Lett.* **80**, 4402 (1998), ISSN 0031-9007.
 - [6] T. Takekoshi, B. M. Patterson, and R. J. Knize, *Phys. Rev. Lett.* **81**, 5105 (1998), ISSN 0031-9007.
 - [7] L. D. Carr, D. DeMille, R. V. Krems, and J. Ye, *New Journal of Physics* **11**, 055049 (2009), URL <http://stacks.iop.org/1367-2630/11/i=5/a=055049>.
 - [8] O. Dulieu, R. Krems, M. Weidemuller, and S. Willitsch, *Phys. Chem. Chem. Phys.* **13**, 18703 (2011), URL <http://dx.doi.org/10.1039/C1CP90157E>.
 - [9] G. Quémener and P. S. Julienne, *Chemical Reviews* **112**, 4949 (2012), URL <http://dx.doi.org/10.1021/cr300092g>.
 - [10] D. W. Chandler, *The Journal of Chemical Physics* **132**, 110901 (2010), URL <http://scitation.aip.org/content/aip/journal/jcp/132/11/10.1063/1.3357286>.
 - [11] S. Ospelkaus, K.-K. Ni, D. Wang, M. H. G.

- de Miranda, B. Neyenhuis, G. Quémener, P. S. Julienne, J. L. Bohn, D. S. Jin, and J. Ye, *Science* **327**, 853 (2010), ISSN 0036-8075, <http://science.sciencemag.org/content/327/5967/853.full.pdf>, URL <http://science.sciencemag.org/content/327/5967/853>.
- [12] M. de Miranda, A. Chotia, B. Neyenhuis, D. Wang, G. Quémener, S. Ospelkaus, J. Bohn, J. Ye, and D. Jin, *Nature Physics* **7**, 502 (2011).
- [13] C. Chin, R. Grimm, P. Julienne, and E. Tiesinga, *Rev. Mod. Phys.* **82**, 1225 (2010), URL <http://link.aps.org/doi/10.1103/RevModPhys.82.1225>.
- [14] M. De Miranda, A. Chotia, B. Neyenhuis, D. Wang, G. Quémener, S. Ospelkaus, J. Bohn, J. Ye, and D. Jin, *Nature Phys.* **7**, 502 (2011).
- [15] J. N. Byrd, J. A. Montgomery, and R. Côté, *Phys. Rev. Lett.* **109**, 083003 (2012), URL <http://link.aps.org/doi/10.1103/PhysRevLett.109.083003>.
- [16] A. J. Leggett, *Rev. Mod. Phys.* **73**, 307 (2001), URL <http://link.aps.org/doi/10.1103/RevModPhys.73.307>.
- [17] S. Giorgini, L. P. Pitaevskii, and S. Stringari, *Rev. Mod. Phys.* **80**, 1215 (2008), URL <http://link.aps.org/doi/10.1103/RevModPhys.80.1215>.
- [18] T. Kraemer, M. Mark, P. Waldburger, J. G. Danzl, C. Chin, B. Engeser, A. D. Lange, K. Pilch, A. Jaakkola, H.-C. Nägerl, et al., *Nature* **440**, 315 (2006), arXiv:cond-mat/0512394.
- [19] D. Shu, I. Simbotin, and R. Côté, *Chem. Phys. Chem.* **17**, 3655 (2016), URL <http://dx.doi.org/10.1002/cphc.201600971>.
- [20] D. DeMille, *Phys. Rev. Lett.* **88**, 067901 (2002), URL <http://link.aps.org/doi/10.1103/PhysRevLett.88.067901>.
- [21] S. F. Yelin, K. Kirby, and R. Côté, *Phys. Rev. A* **74**, 050301 (2006), URL <http://link.aps.org/doi/10.1103/PhysRevA.74.050301>.
- [22] E. Kuznetsova, R. Côté, K. Kirby, and S. F. Yelin, *Phys. Rev. A* **78**, 012313 (2008), URL <http://link.aps.org/doi/10.1103/PhysRevA.78.012313>.
- [23] I. Simbotin, S. Ghosal, and R. Côté, *Phys. Chem. Chem. Phys.* **13**, 19148 (2011), URL <http://dx.doi.org/10.1039/C1CP21982K>.
- [24] J. Wang, J. N. Byrd, I. Simbotin, and R. Côté, *Phys. Rev. Lett.* **113**, 025302 (2014), URL <http://link.aps.org/doi/10.1103/PhysRevLett.113.025302>.
- [25] I. Simbotin and R. Côté, *New Journal of Physics* **17**, 065003 (2015), URL <http://stacks.iop.org/1367-2630/17/i=6/a=065003>.
- [26] I. Simbotin, S. Ghosal, and R. Côté, *Phys. Rev. A* **89**, 040701 (2014), URL <http://link.aps.org/doi/10.1103/PhysRevA.89.040701>.
- [27] I. Simbotin and R. Côté, *Chemical Physics* **462**, 79 (2015), ISSN 0301-0104, inelastic Processes in Atomic, Molecular and Chemical Physics, URL <http://www.sciencedirect.com/science/article/pii/S0301010415001834>.
- [28] I. Simbotin and R. Côté, *J. Phys. B* (2017), URL <https://doi.org/10.1088/1361-6455/aa6821>.
- [29] A. B. Henson, S. Gersten, Y. Shagam, J. Narevicius, and E. Narevicius, *Science* **338**, 234 (2012), 1208.1681.
- [30] E. Lavert-Ofir, Y. Shagam, A. B. Henson, S. Gersten, J. Klos, P. S. Żuchowski, J. Narevicius, and E. Narevicius, *Nature Chem.* **6**, 332 (2014).
- [31] Y. Shagam, A. Klein, W. Skomorowski, R. Yun, V. Averbukh, C. P. Koch, and E. Narevicius, *Nature Chem.* **7**, 921 (2015).
- [32] A. Klein, Y. Shagam, W. Skomorowski, P. S. Żuchowski, M. Pawlak, L. M. C. Janssen, N. Moiseyev, S. Y. T. van de Meerakker, A. van der Avoird, C. P. Koch, et al., *Nature Phys.* (2016), doi:10.1038/nphys3904.
- [33] J. Taylor, *Scattering Theory: The Quantum Theory of Nonrelativistic Collisions*, Dover Books on Engineering (Dover Publications, 2012), ISBN 9780486142074.
- [34] R. Newton, *Scattering Theory of Waves and Particles*, Dover Books on Physics (Dover Publications, 1982), ISBN 9780486425351.
- [35] C. Joachain, *Quantum collision theory* (North-Holland, 1975), ISBN 9780720402940.
- [36] N. Balakrishnan, V. Kharchenko, R. Forrey, and A. Dalgarno, *Chemical Physics Letters* **280**, 5 (1997), ISSN 0009-2614, URL <http://www.sciencedirect.com/science/article/pii/S000926149701052X>.
- [37] E. P. Wigner, *Phys. Rev.* **73**, 1002 (1948), URL <http://link.aps.org/doi/10.1103/PhysRev.73.1002>.
- [38] E. Bodo, F. A. Gianturco, N. Balakrishnan, and A. Dalgarno, *J. Phys. B* **37**, 3641 (2004), URL <http://stacks.iop.org/0953-4075/37/i=18/a=007>.
- [39] M. T. Cvitas, P. Soldan, J. M. Hutson, P. Honvault, and J.-M. Launay, *The Journal of Chemical Physics* **127**, 074302 (2007).
- [40] D. Skouteris, J. Castillo, and D. Manolopoulos, *Computer Physics Communications* **133**, 128 (2000), ISSN 0010-4655, URL <http://www.sciencedirect.com/science/article/pii/S0010465500001673>.
- [41] N. Balakrishnan, *Journal of Chemical Sciences* **124**, 311 (2012), ISSN 0973-7103, URL <http://dx.doi.org/10.1007/s12039-012-0230-8>.
- [42] W. Bian and H.-J. Werner, *The Journal of Chemical Physics* **112**, 220 (2000), URL <http://scitation.aip.org/content/aip/journal/jcp/112/1/10.1063/1.480574>.
- [43] K. Stark and H. J. Werner, *The Journal of Chemical Physics* **104**, 6515 (1996), URL <http://scitation.aip.org/content/aip/journal/jcp/104/17/10.1063/1.471372>.
- [44] N. Balakrishnan and A. Dalgarno, *Chemical Physics Letters* **341**, 652 (2001), ISSN 0009-2614, URL <http://www.sciencedirect.com/science/article/pii/S0009261401005152>.
- [45] A. I. Boothroyd, W. J. Keogh, P. G. Martin, and M. R. Peterson, *The Journal of Chemical Physics* **104**, 7139 (1996), URL <http://scitation.aip.org/content/aip/journal/jcp/104/18/10.1063/1.471430>.
- [46] K. Willner and F. A. Gianturco, *Phys. Rev. A* **74**, 052715 (2006), URL <http://link.aps.org/doi/10.1103/PhysRevA.74.052715>.